International Journal of Nanoelectronics and Materials
Volume 12, No. 1, Jan 2019 [1-10]

Annealing Effects on Band Tail Width, Urbach Energy and Optical Parameters of Fe_2O_3:Ni Thin Films Prepared by Chemical Spray Pyrolysis Technique

N. N. Jandow[1*], N. F. Habubi[1], S. S. chiad[1], I. A. Al-Baidhany[1] and M. A. Qaeed[2]

[1]*Department of Physics/College of Education/ Mustansiriyah University/Baghdad- Iraq.*
[2]*Physics Department/Faculty of Science, Jeddah University/Saudi Arabia, Jeddah.*

Received 20 November 2017; Revised 7 July 2018; Accepted 17 July 2018

ABSTRACT

In this research, nickel doped Iron oxide (Fe_2O_3:Ni) thin films were deposited onto glass substrates by using chemical spray pyrolysis (CSP) technique. The deposited films thickness was found to be about 350±30 nm. The films were annealed at two different temperatures (450 °C and 500°C). The X-ray Diffraction spectra (XRD) results indicate that the structure of the three prepared thin films was polycrystalline in nature and has a hexagonal phase with preferred orientation along (104) plane. Temperature annealing effects on the optical properties of the deposited films was studied. It was found that, the optical parameters, such as the refractive index (n), the real (ε_1) and imaginary (ε_2) parts of dielectric constant which related to n, Urbach energy and the energy gap; all depend on the annealing temperature. The results show that there was a reduction in the optical absorbance as well as the dielectric constants. The dispersion parameters decreased with the increasing annealing temperature while the determined Urbach energy was increased. The optical energy gap decreased from 2.74 to 2.67 eV with the increasing annealing temperature, on the account that there is an inverse relation between Urbach energy and energy gap.

Keywords: Fe_2O_3:Ni, Structural Properties, Optical Properties, Dispersion Parameters, Urbach Energy, Chemical Spray Pyrolysis.

1. INTRODUCTION

Hematite (α–Fe_2O_3) is a material with a band gap of about 2-2.2eV allowing the absorption of ~40% solar energy via its visible area. Due to this factor, Fe_2O_3 is considered as a promising material for solar energy application. Fe_2O_3 is low cost due to its abundance in nature and it also behave as corrosion-resistant in acidic and alkaline media [1]. This metal oxide has found its way for many other applications according to its dielectric properties and its breakthrough having at once high thermopower [2-7].

However, some major efforts have been done in the fabrication of a Fe_2O_3 photoanode as well as electrocatalyst, such as low electrical conductivity of the material itself and the necessity of having less than 5 nm particle synthesis as to prevent electron-hole recombination related to the extremely short diffusion distance of holes, among others [8]. By impurity doping, its resistivity can be lowered and considerations of the diffusion length of minority carriers have indicated that p-type Fe_2O_3 could be a better photoanode [9]. Many researchers have been using different techniques for depositing Fe_2O_3 such as; colloidal chemistry method [10], sol-gel [11], usual ceramic technique [12], spray pyrolytic method [13-14], spin coating solution deposition

* Corresponding Author: *nidhaljandow@uomustansiriyah.edu.iq*

[15], sputtering [16], pulsed laser deposition [17], and molecular beam epitaxy [18]. Different physical parameters have been studied for this metal oxide material such as the optical and structural parameters.

From the literature, and to our best knowledge, there is no study about the effects of annealing temperature on the optical parameters such as the dispersion parameters and Urbach energy of Fe_2O_3:Ni thin films prepared by utilizing the chemical spray pyrolysis (CSP) technique. In this work, we investigate the effects of annealing temperatures (400, and 500ºC) on the optical parameters of the deposited Fe_2O_3:Ni thin films by using the chemical spray pyrolysis (CSP) technique.

2. RESERCH METHODOLOGY

Ni-doped Fe_2O_3 thin films was prepared using CSP technique. A homemade glass atomizer was used to spray the solution. The films were deposited onto cleaned glass slides substrates heated to 400°C. The initial solution was including a 0.1M of $FeCl_3$ (Somatco Supplies Chemicals, India) and 0.1M of $NiCl_2$ (Spectrum Chemicals, India) diluted with redistilled water to obtain an aqueous solution. Few drops of HCl were added in order to obtain a clear solution during the deposition. The volumetric concentration of Ni content was 3%. The optimum conditions was achived at the following condition: spraying rate was about 4 ml/min, spraying time was 7 seconds lasted by (1.5 minutes) to avoid any excessive cooling, the air carrier gas (at a pressure of 10^5 Pascals), and the distance between the nozzle and the substrate was about 28±1 cm.

Film thickness was measured by gravemetric method and it was found that the thickness was in the range of 350±30 nm. The prepared films were annealed at different temperatures (450 and 500ºC). The optical transmittance and absorbance spectra were recorded in the wavelength range of 380-900 nm by using double beam UV-Visible spectrophotometer (Shimadzu UV probe 1650, Japan).

The average crystallite size (D) of the hematite films was determined by using Scherrer formula [19].

$$D = \frac{K\lambda}{B\cos\theta} \tag{1}$$

where B is the FWHM (in radians) of X-ray Diffraction spectra (XRD) intensity, λ is the X-ray wavelength (Cu Kα =0.154 nm), θ is the Bragg diffraction angle, and K is the shape factor which is taken as 0.9.

To determine the total defects in the films, the dislocation density (δ) was calculated using the relation [19]:

$$\delta = \frac{1}{D^2} \tag{2}$$

The micro strain (ε) of the deposited film on the substrate was calculated using the relation [19]:

$$\varepsilon = \frac{\beta\cos\theta}{4} \tag{3}$$

The real (ε_1) and imaginary (ε_2) parts of dielectric constant are related to the refractive index (n) and extinction coefficient (K) values. The ε_1 and ε_2 values were calculated using the formulas in (4) and (5) [20]:

$$\varepsilon_1 = n^2 - K^2 \tag{4}$$

$$\varepsilon_2 = 2nK \tag{5}$$

The amplitude of the electromagnetic wave reduced by a factor of *e* after passing through a known thickness called a skin depth (x) which can be calculated by the following relation [21]:

$$x = \frac{\lambda}{2\pi k} \tag{6}$$

In the exponential edge region, the Urbach rule is expressed as [22]:

$$A = \alpha_o \exp(h\upsilon/E_U) \tag{7}$$

where α_o is a constant, E_U is the Urbach energy that characterizes the slope of the exponential edge, and $h\upsilon$ is the photon energy.

In order to estimate the refractive index dispersion of the films, the single-oscillator model developed by DiDomenico and Wemple [23] was used. In terms of the dispersion energy (E_d) and single-oscillator energy (E_o), the single-oscillator model for the refractive index dispersion is expressed as follows [23]:

$$n^2 - 1 = \frac{E_o\, E_d}{E_o^2 - E^2} \tag{8}$$

where E_d and E_o are single oscillator parameters. E_o is the single oscillator energy while E_d is the so-called dispersion energy which measures the average strength of interband optical transitions, and E is the photon energy ($h\upsilon$).

The oscillator energy (E_o) is an average of the optical band gap (E_g) [24] and can be obtained by an empirical formula to the optical band gap value:

$$E_o = 2E_g \text{ [25].} \tag{9}$$

The static refractive index, n(0) was evaluated from the equation ($n(0) = 1 + E_d/E_o$) and the value of the static dielectric constant ($\varepsilon_\infty = n^2(0)$) was calculated. The dispersion data of refractive index can be estimated according to the following relation[26]:

$$n^2 - 1 = \frac{S_o\, \lambda_o^{\;2}}{1 - (\lambda_o/\lambda)^2} \tag{10}$$

Thus, the determination of the moments (M_{-1} and M_{-3}) of the ε_i spectrum is very important for the optical applications. M_{-1} and M_{-3} can be obtained from the following relations [27]:

$$E_o^2 = \frac{M_{-1}}{M_{-3}} \tag{11}$$

$$E_d^2 = \frac{M_{-1}^3}{M_{-3}} \tag{12}$$

3. RESULTS AND DISCUSSIONS

Figure 1 shows three XRD diffraction patterns of the deposited Fe_2O_3:Ni thin films on glass substrates. Figure 1(a) shows the XRD diffraction patterns after annealing with 450ºC, Figure 1(b) is the pattern for before annealing and Figure 1(c) is the patterm obtained after annealing with 500ºC. with 2θ peak referred to (012), (104), (110) and (116) direction respectively. By comparing the 2θ peak direction to the International Center for Diffraction Data (ICDD), it is clear that the preferred orientation for the three films is in the (104) direction indicating that the films has a hexagonal phase. These results were in good agreement with the results reported by Ubale and Belkhedkar [19]. The figures show that for the three deposited films; the strong peak value corresponds to (104) direction located at 2θ=33.175, 33.225 and 33.275 with full width at half maximum intensity (FWHM) of 0.45, 0.30 and 0.25 respectively, while the (012, 110 and 116) peaks values are lower intensity than the (104) peak. The figures also show that as the annealing temperature increases while the FWHM decreases, the diffraction peaks become sharper and their intensity is enhanced; this indicates that the film structure improved as the annealing temperature increased.

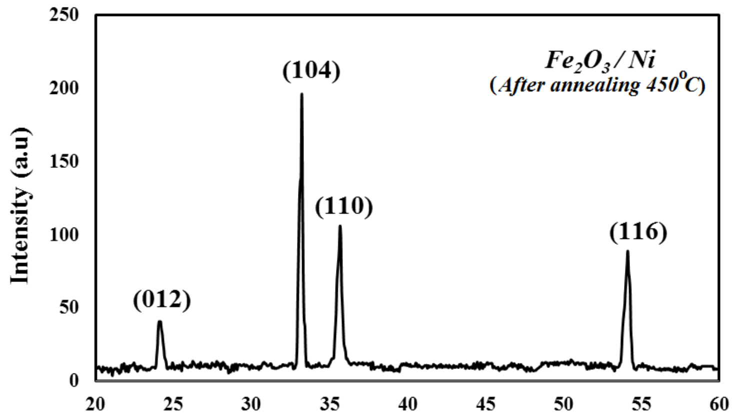

(a)

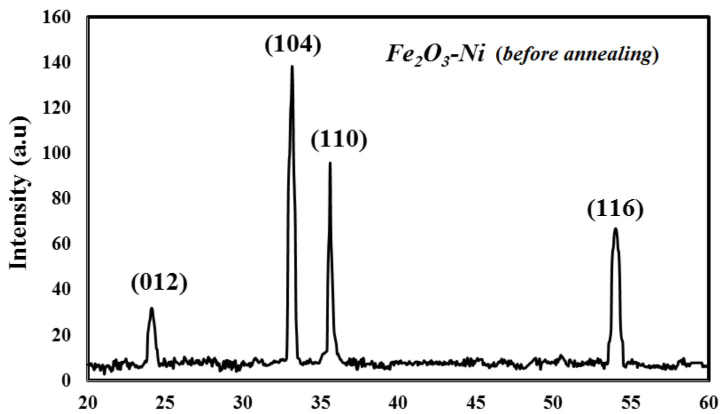

(b)

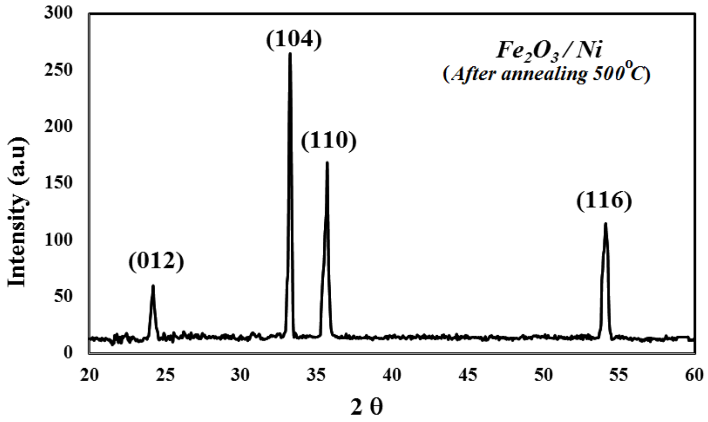

(c)

Figure 1. XRD patterns of Fe_2O_3:Ni thin films (a) after annealing at 450ºC, before annealing and after annealing at 500ºC.

By using Scherrer formula (Equation1), the value from the prominent peak (104) increased as the annealing temperature increases indicating that the crystalline quality of the film is improved. It is found that for the smaller crystallite size, the dislocation density is higher and it decreases as crystallite size increases. It is very natural that, when the crystallite size increases and the grain boundaries density decreases; this means that the crystallinity of the thin films is improved.

The micro strain provides the information about the defects present around the lattice. The variation of crystallite size, dislocation density and micro strain values for Fe_2O_3:Ni films deposited before and after annealing at 450 and 500ºC are listed in Table 1.

Table 1 X-ray diffraction data summary for the preferential orientation (104) direction for Fe_2O_3:Ni thin films before and after annealing at 450 and 500ºC

Fe_2O_3/Ni	2θ (°)	Peak intensity	FWHM (°)	Crystallite Size (nm)	Dislocation density (δ) (10^{-4} nm^{-1})	Micro Strain (ε)×10^{-2}
Before annealing	33.175	138.513	0.450	18.225	30.106	10.780
Annealing (450°C)	33.225	198.273	0.300	27.340	13.378	7.186
Annealing (500°C)	33.275	264.712	0.250	32.811	0.928	5.988

The absorption spectra of the three deposited Fe_2O_3:Ni thin films before and after annealing with 450 and 500ºC are shown in Figure 2. From the figure, it can be seen that the absorbance decreases with wavelength and has relatively low values in the visible (after 550 nm) and IR regions of the spectrum. The result indicates that there is a very small amount optical absorption in the visible region compared to the UV region, hence the film has a potential application in the fabrication of solar cell and UV photodetector The results show that the absorbance increases as the annealing temperature decreses.

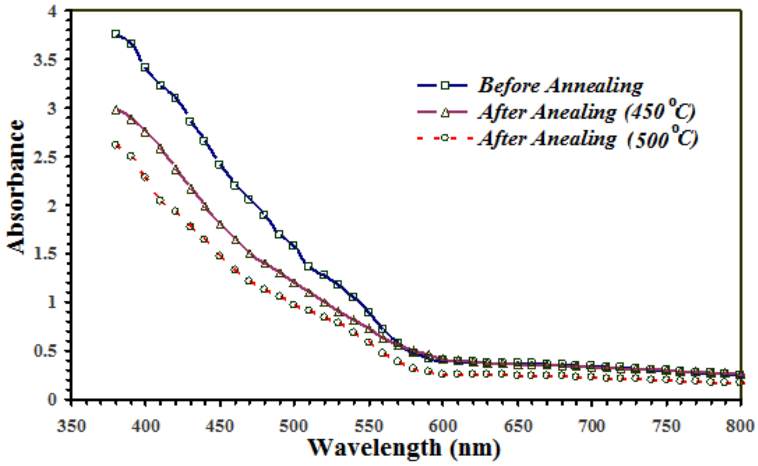

Figure 2. Absorbance spectra of Fe_2O_3:Ni thin films before and after annealing at 450 and 500°C.

The ε_1 and ε_2 values, dependence of wavelength are respectively shown in Figures 3 and 4. From the two figures, notice that the ε_1 values are higher than that of ε_2 values. The ε_1 and ε_2 values decrease with the increasing of annealing temperatures. The decrease in refractive index could be attributed to the increase of homogeneity of Fe_2O_3:Ni films with annealing temperature.

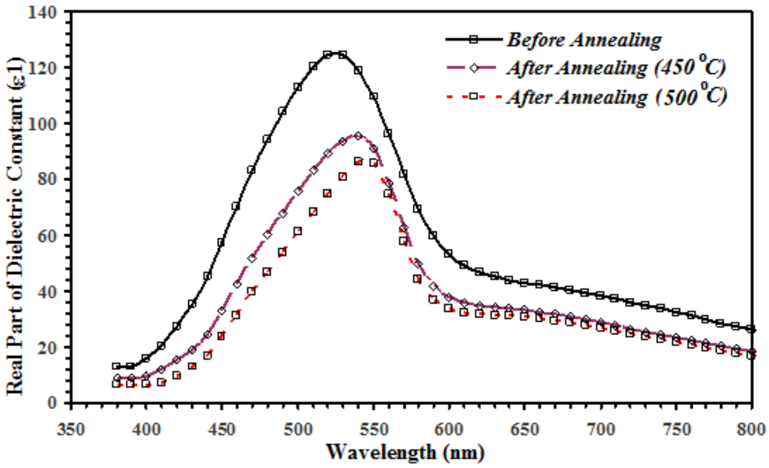

Figure 3. Plot of the real part of the dielectric constant for Fe_2O_3:Ni thin films before and after annealing at 450 and 500°C.

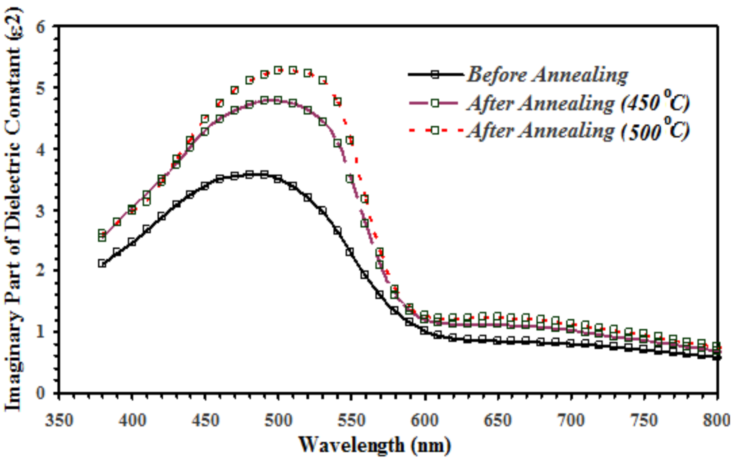

Figure 4. Plot of the imaginary part of the dielectric constant for Fe_2O_3:Ni thin films before and after annealing at 450 and 500°C.

The skin depth can take the value of one hundred to several thousands angstrom depending on the characteristics of the material. Figure 5 shows the variation of skin depth versus wavelength. It can be seen that; at shorter wavelengths there is no change in their values before and after annealing. This might be due to the absorption of equal probability in this region, but after wavelength, λ *(cut off)* (~520nm) the skin depth values became larger as the annealing temperature increases.

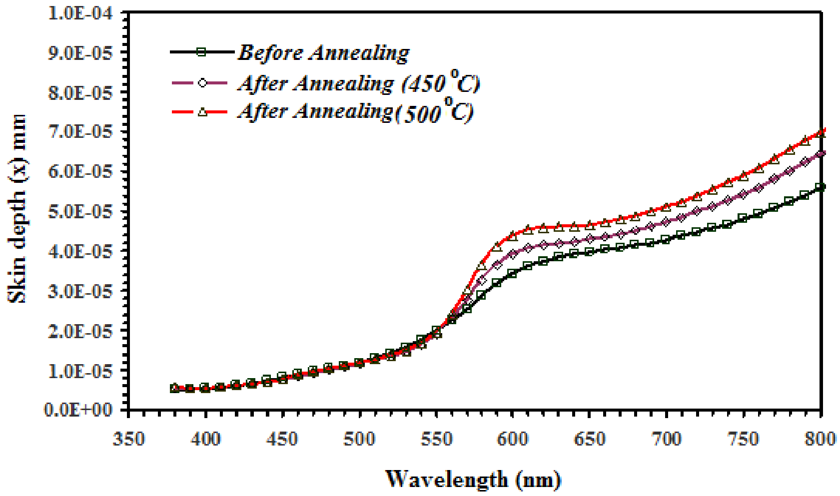

Figure 5. Plot of skin depth for Fe_2O_3:Ni thin films before and after annealing at 450 and 500°C.

Equation (7) describes the optical transition between occupied states in the valence band tail to the unoccupied states of the conduction band edge. The value of E_U was obtained from the reciprocal of the slope of lnα vs. hν as shown in Figure 6 and listed in Table 2. It can be seen that there is an inverse relation between energy gap and Urbach energy. The decrease in the optical enegy gap is attributed to the increase of disorder of the material due to doping[28].

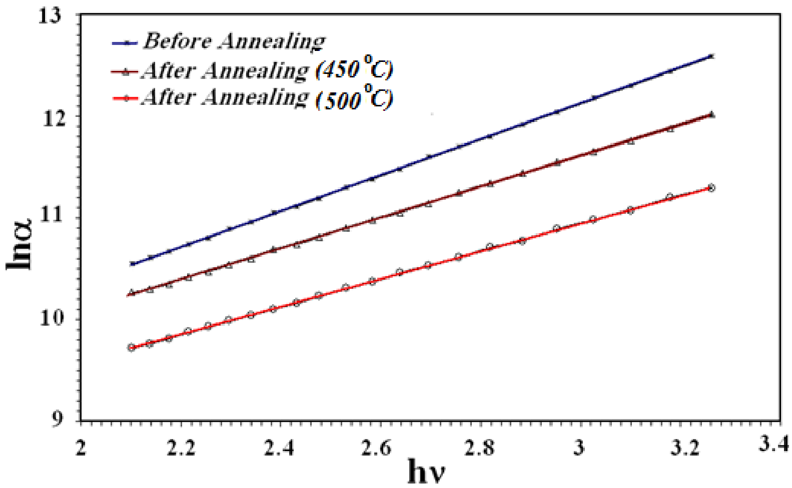

Figure 6. Ln (α) vs (hυ) for Fe_2O_3:Ni thin films before and after annealing at 450 and 500°C.

From Equation (8) and by plotting $(n^2-1)^{-1}$ vs. $(h\upsilon)^2$ as illustrated in Figure 7; E_o and E_d values were determined from the slope $(E_oE_d)^{-1}$and intercept (E_o/E_d) on the vertical axis respectively and their values were calculated from the plot of $(n^2-1)^{-1}$vs. $(1/\lambda^2)$ as shown in Figure 8.

Table 2 summarizes the values of E_o, E_d, n(0), ε_∞, S_o and λ_o for the as-deposited and annealed Fe_2O_3:Ni thin films.

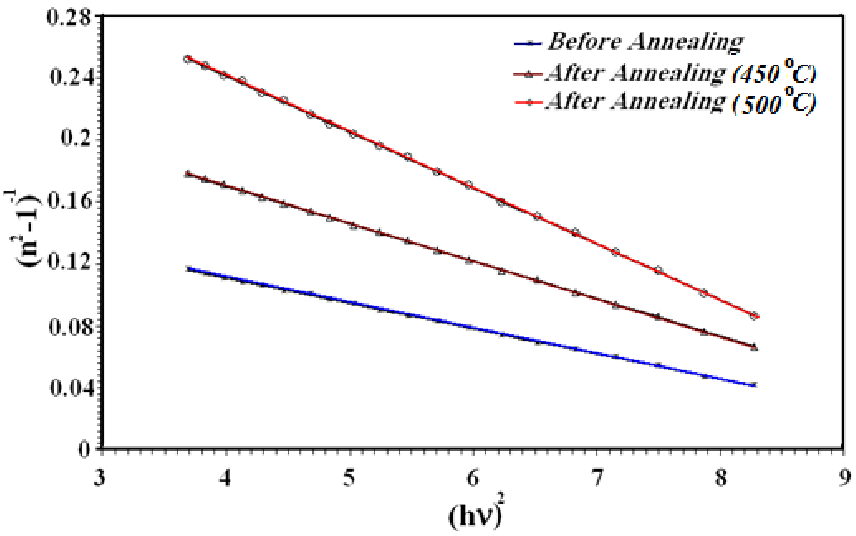

Figure 7. $(n^2-1)^{-1}$ versus $(h\upsilon)^2$ for Fe_2O_3:Ni thin films before and after annealing at 450 and 500°C.

The single-oscillator parameters E_o and E_d is related to the imaginary of ε_i of the complex dielectric constant. The ε_i parameter includes the desired response information about the electronic and optical properties of the used material. It was found that their values decrease as the annealing temperature increases as shown in Table 2. This might be due to the dependence of these moment on the complex dielectric constant[29].

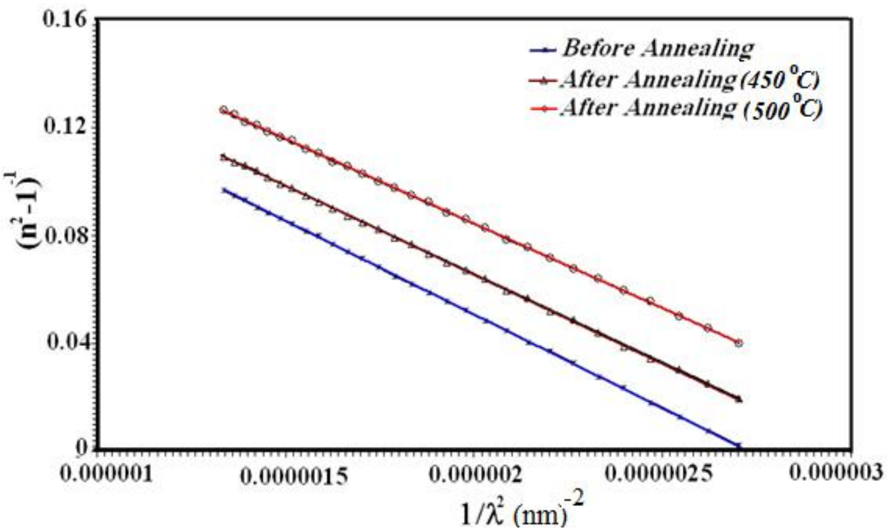

Figure 8. $(n^2-1)^{-1}$ versus $(1/\lambda^2)$ for Fe_2O_3:Ni thin films before and after annealing at 450 and 500°C.

Table 2 The optical parameters of Fe_2O_3:Ni thin films for different annealing temperatures

Sample	E_d (eV)	E_o (eV)	E_g (eV)	ε_∞	n(o)	M_{-1}	M_{-3} (eV^{-2})	S_o x10^{13} (m^{-2})	λ_o (nm)	U_E (meV)
Before annealing	43.8	5.70	2.85	8.69	2.94	7.69	0.236	2.89	588	451
After annealing (450 °C)	30.0	5.48	2.74	6.55	2.56	5.55	0.185	3.08	519	523

After annealing (500 ^{o}C)	20.5	5.34	2.67	4.84	2.20	3.84	0.134	3.20	472	595

4. CONCLUSION

Fe_2O_3:Ni thin films have been deposited by spray pyrolysis technique on glass substrate with 3% doping of Ni. XRD pattern reveals that all the deposited films were polycrystalline with a preferred orientation along (104) plane. It was found that the optical absorbance decreased as well as the dielectric constants and dispersion parameters such as E_d, E_o, ε_∞, n(0), λ_o, M_{-1}, and M_{-3} decreased with increasing annealing temperature in contrary with the values of S_o. The determined Urbach energy increased and the energy gap decreased from 2.74 to 2.67 eV with the increasing of annealing temperature.

ACKNOWLEDGEMENT

This research did not receive any specific grant from funding agencies in the public, commercial, or not-for-profit sectors.

REFERENCES

[1] I.A. Raid, Y. Najim, M. Ouda, Spray Pyrolysis Deposition of α Fe_2O_3 Thin Film, e-J. Surf. Sci. Nanotech. **6** (2008) 96-98.
[2] D. G. Wang, C. Z. Chen, J. Ma, T. H. Liu Lead-based titanate ferroelectric thin films fabricated by a sol-gel technique, App. Surf. Sci. **255** (2008) 1637-1645.
[3] D. Biprodas, F. A. Niveen, P. L. Ian, Effect of mixed transition-metal ions in glasses. I. The P_2O_5–V_2O_5–Fe_2O_3 system, J. Non-Cryst. Solids. **351**, 24-26 (2005) 1958-1966.
[4] N. F. Habubi, K. A. Mishjil, H. G. Rashid, Theortical estimation of direct transitions of Fe [subíndice 2] O [subíndice 3] thin film, Atti. Dell. Fond Gior. Ron. **66**, 6 (2011) 883-891.
[5] N. J. Mohmmed, N. F. Habubi, Structural and Optical Properties of Fe_2O_3-NiO mixed Thin Films Prepared by Chemical Spray Pyrolysis, Int. lett. Chem. Phys. astron. **14**, 1 (2014) 65-85.
[6] T. Bak, J. Nowotny, M. Rekas, C. C. SorrellInt, Review: Photo-electrochemical hydrogen generation from water using solar energy. Materials-related aspects, J. Hydrogen Energ. **27** (2002) 991-1022.
[7] A. L. Stroyuk, I. V. Sobran, S. Y. Kuchmiy, Photoinitiation of acrylamide polymerization by Fe_2O_3 nanoparticles, J. Photoch. Photobio. A. **192**, 2-3 (2007) 98-104.
[8] S. Kuang, L. Yang, S. Luo, Q. Cai, Fabrication, characterization and photoelectrochemical properties of Fe_2O_3 modified TiO_2 nanotube arrays, Appl. Surf. Sci. **255**, 16 (2009)7385-7388.
[9] C. C. Leygraf, M. Hendewek, A. G. Somarjoi, The Preparation and Selected Properties of Mg-Doped p-Type Iron Oxide as a Photocathode for the Photoelectrolysis of Water Using Visible Light, J. Solid State Chem. **48** (1983) 357-367.
[10] S. Musić, S. Popović, S. Dalipi, Formation of oxide phases in the system Fe_2O_3 NiO, J. Mater. Sci. **28**, 7 (1993)1793-1798.
[11] S. Solinas, G. Piccaluga, M. P. Morales, C. J. Serna, Sol-gel formation of γ Fe_2O_3/SiO_2 nanocomposites, Acta mater. **49** (2001) 2805-2811.
[12] S. Mohanty & J. Ghose, Studies on Some α-Fe_2O_3 Photoelectrodes, J. Phys. Chem. Solids. **53**, 1 (1992) 81-91.

[13] N. Khademi, M. M.Bagheri-Mohagheghi, The Structural, Thermoelectric and Optical Properties of SnO_2-Fe_2O_3: Bi Thin Films Deposited by Spray Prolysis Technique, T.E.P.E. **2**, 3 (2013) 89-93.
[14] J. D. Desai, H. M.Pathan, S. K. Min, K. D. Jung, O. S. Joo, Preparation and Characterization of Iron Oxide Thin Films by Spray Pyrolysis using Methanolic and Ethanolic Solutions, App. Surf. Sci. **252** (2006)2251-225
[15] F. L. Souza, K. P. Lopes, E. Longo, E. R. Leite, The influence of the film thickness of nanostructured alpha-Fe_2O_3 on water photooxidation, Phys. Chem. Phys. **11** (2009) 1215-1219
[16] J. Chavez-Galan, R. Almanza, Solar filters based on iron oxides for energy savings with efficient windows, Sol. Energ. **81**, 1 (2007) 13-19.
[17] M. G. Chapline & S. X. Wang, Observation of the Verwey transition in thin magnetite films, J. Appl. Phys. **97**, 12 (2005)123901-3.
[18] S. k. Arora, G. R. S. Sumesh, I. Shvets, M. Luysberg, Anomalous strain relaxation behavior of Fe_3O_4/MgO (100) heteroepitaxial system grown using molecular beam epitaxy, J. Appl. Phys. **100** (2006) 3908-073908.
[19] A. U. Ubale & M. R. Belkhedkar, Size Dependent Physical Properties of Nanostructured α-Fe_2O_3 Thin Films Grown by Successive Ionic Layer Adsorption and Reaction Method for Antibacterial Application, J. Mater. Sci. Technol. **31**, 1 (2015)1-9.
[20] S. Moss, J. G. Burrell, B. Ellis, Semiconductor Opto-Electronics, Wiley, New York, (1973).
[21] J. F. Eloy, Power Lasers, National School of Physics, Grenoble, France, John Wiley & Sons, (1984).
[22] J. Tauc, Amorphous and Liquid Semiconductors, Plenum Press, New York, (1974).
[23] M. DiDomenico & S. H. Wemple, Oxygen-Octahedra Ferroelectrics. I. Theory of Electro-Optical and Nonlinear-Optical Effects, J. Appl. Phys. **40** (1969) 720-734.
[24] H. S. Wemple & M. Didomenico, Behavior of the Electronic Dielectric Constant in Covalent and Ionic Materials, Phys. Rev. B. **3** (1971)1338-1351.
[25] M. Modreanu, M. Gartner, N. Tomozeiu, J. Seekamp, P. Cosmin, Investigation on optical and microstructural properties of photoluminescent LPCVD SiO_xN_y thin films, Opt. Mater. **17** (2001)145-148.
[26] A. F. Quasrawi & M. M S. Ahmad, Optoelectronical properties of polycrystalline β-GaSe thin films, Cryst. Res. Technol. **41**(2006) 364-370.
[27] S. H. Wemple & M. DiDomenico, Optical Dispersion and the Structure of Solids, Phys. Rev. Lett. 23 (1969)1156-1160.
[28] Saliha Ilican,Yasemin Caglar, Mujdat Caglar, Faherettin Yakuphanoglu,Structural ,optical and electrical properties of F-doped ZnO nanrod semiconductor thin films deposited by dol-gel process,Applied Surface Science **255** (2008) 2353-2359.
[29] Mujdat Caglar, Saliha Ilican, Yasemin Caglar, Structural mmorphological and optical properties of $CuAlS_2$ films deposited by spray pyrolysis method, Optics Communications **281** (2008) 1615-1624.